ADVANCED MATERIALS
www.advmat.de

Non-Equilibrium Assembly of Light-Activated Colloidal Mixtures

Dhruv P. Singh, Udit Choudhury, Peer Fischer, and Andrew G. Mark**

The collective phenomena exhibited by artificial active matter systems present novel routes to fabricating out-of-equilibrium microscale assemblies. Here, the crystallization of passive silica colloids into well-controlled 2D assemblies is shown, which is directed by a small number of self-propelled active colloids. The active colloids are titania–silica Janus particles that are propelled when illuminated by UV light. The strength of the attractive interaction and thus the extent of the assembled clusters can be regulated by the light intensity. A remarkably small number of the active colloids is sufficient to induce the assembly of the dynamic crystals. The approach produces rationally designed colloidal clusters and crystals with controllable sizes, shapes, and symmetries. This multicomponent active matter system offers the possibility of obtaining structures and assemblies that cannot be found in equilibrium systems.

A promising approach to the development of new structures and materials is self-assembly, in which functional microscopic entities organize into defined configurations.[1–5] Successful implementations have been based on DNA recognition,[1,2] shape selectivity,[3] and surface functionalization[4,6] where in these cases the end state structures are defined by local or global thermodynamic minima. Another way is to pursue out-of-equilibrium dynamic assembly and self-organization of the sort characteristic of many living systems. Phenomena such as flocking and schooling arise when self-propulsive, out-of-equilibrium actors interact with one another.[7–11] At the microscale, motile bacteria, particularly *Escherichia coli*, exhibit organizational behaviors ranging from simple pairwise alignment and aggregation into swarms,[12,13] to complex transport of other nonmotile species in a symbiotic strategy to detoxify their environment.[14] Artificial active systems promise not only insights into living systems, but offer an unconventional route to self-assembling structures and materials. In this work, we harness active particles to assemble hybrid clusters, crystals, and glasses whose symmetry and size can be dynamically controlled.

Recent work has shown that artificial active matter systems exhibit emergent collective behaviors that are as rich as the biological systems that inspired them.[15–23] Typical active systems include Quincke rollers,[15] electrophoretically driven Janus particles,[22] and catalytic micromotors which propel by chemically decomposing their local environment.[24–29] One of the important phenomena that these systems display is the coalescence of particles into crystals—ordered arrays with translational symmetry. Palacci et al. have, for instance, shown crystal formation with giant number fluctuations in light-activated colloidal (Fe_2O_3-TPM) particles in aqueous peroxide solution.[17] Similarly, Buttinoni et al. demonstrated dynamic cluster growth of light-active Janus particles (carbon–SiO_2) in a water–lutidine binary mixture.[18] In these examples, all of the particles were active. On the other hand, mixed systems, which combine active with nonmotile species have been much less studied. In some cases, the active particles have been seen to collect the passive particles,[30,31] for instance Ibele et al. described a "predator–prey" relationship between AgCl active particles hunted by passive particles.[16] Meanwhile, theory has predicted that a small fraction of active colloids can promote condensation in passive hard-sphere glasses,[32] and that a small fraction of active colloids can induce phase separation and self-assembly in passive colloids.[33]

Here, we show that a few active, self-propelled colloids can drive the self-assembly of many passive spectator particles to form large 2D assemblies. The twin consequences of active self-propulsion and attraction of nearby passive particles are diffusiophoretic effects arising from a local chemical gradient activated by UV illumination. One benefit to this actively driven assembly scheme is that the interaction strength can be set and dynamically tuned through the light intensity. Thus, the assembled structures can be tuned from isolated clusters of defined size to extended crystals. Furthermore, the symmetry of the clusters and lattices can be controlled by the size ratio between the passive particles and the active particles that bind them together. We use this approach to construct isolated square, pentagonal, hexagonal, and heptagonal clusters as well as larger assemblies with ordered and disordered translation symmetry. In all cases, the assembly persists until the light is turned off.

Dr. D. P. Singh, U. Choudhury, Prof. P. Fischer, Dr. A. G. Mark
Max-Planck-Institute for Intelligent Systems
Heisenbergstr. 3, 70569 Stuttgart, Germany
E-mail: fischer@is.mpg.de; mark@is.mpg.de
U. Choudhury
Faculty of Mathematics and Natural Sciences
University of Groningen
Groningen, 9747 AG, The Netherlands
Prof. P. Fischer
Institut für Physikalische Chemie
Universität Stuttgart
Pfaffenwaldring 55, 70569 Stuttgart, Germany

DOI: 10.1002/adma.201701328

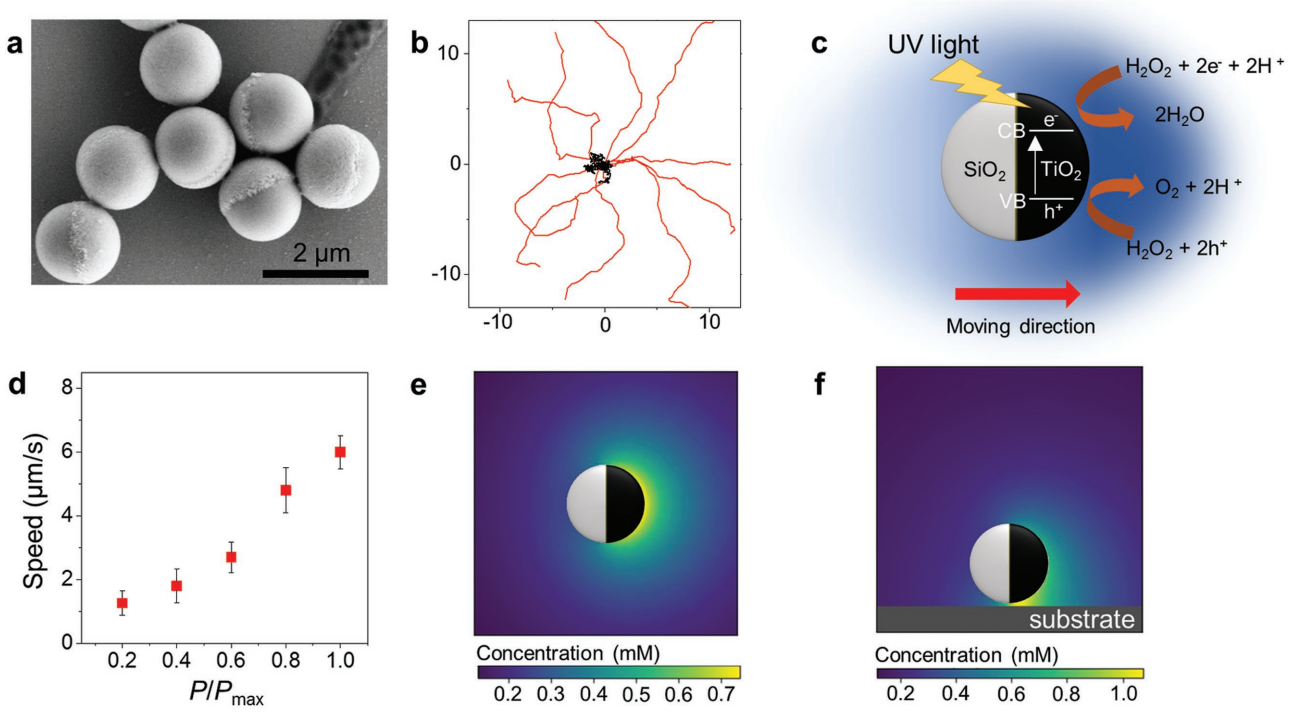

Figure 1. Light-activated self-propelled Janus particles. a) SEM image of light-activated Janus particles showing the TiO_2 cap upon SiO_2 sphere. b) Trajectories of active Janus particles when the UV light is on (red) and off (black) over 3 s acquisition. The units in panel (b) are μm. c) The UV mediated catalytic decomposition of H_2O_2 at the TiO_2 face of the particle. The gradient causes the particle to move by diffusiophoresis toward the TiO_2 surface. d) Average speed of active Janus particles under different light intensities. P_{max} is the maximum light intensity (320 mW cm^{-2}) at our disposal. e,f) Top down (e) and side-view (f) images of the simulated concentration field around a Janus particle in proximity to a substrate.

This multicomponent active matter system offers the possibility of obtaining interesting structures that cannot be found in equilibrium systems, for instance by annealing the structure through changes in the light intensity.

The light-driven, self-propelled colloids are Janus particles composed of SiO_2 and anatase TiO_2 halves (see **Figure 1**a for a scanning electron microscopy (SEM) image and the Experimental Section for more details and the preparation process). We begin by working with particles with a diameter of 1.5 μm. When dispersed in an aqueous hydrogen peroxide solution (H_2O_2 1.5%, pH ≈ 7) they exhibit passive Brownian diffusion in the absence of UV light. However, upon light illumination at 365 nm the Janus colloids show prompt and rapid self-propulsion that on short time scales is ballistic (Figure 1b). The propulsion arises from the photocatalytic decomposition of H_2O_2 at the TiO_2 surface by UV-promoted electron–hole pairs[34–36] (see Figure 1c). The reaction products develop near the TiO_2 hemisphere and thus induce a chemical gradient (O_2 or H_2O_2) between the poles of the Janus colloid, leading to self-phoretic motion of the particle toward the TiO_2 half of the sphere.[25,37–45] Numerical simulations of the diffusion of O_2 product from the active side of the particle confirm that the photocatalytic reaction establishes a local concentration gradient between the two hemispheres of the Janus particle (Figure 1e,f; see also Note 1 in the Supporting Information and the Experimental Section for details). When the light is on, we observe the individual active Janus particles move with a mean speed of 6 μm s^{-1} under neutral pH conditions (Video S1, Supporting Information). Since the rate of photocatalytic decomposition near the TiO_2 surface depends on the intensity of light, the speed of Janus particles increases with UV power (see Figure 1d). Unlike earlier light-activated particles,[17] ours exhibit active propulsion even in the bulk away from the substrate, and orient themselves so that their symmetry axes lie parallel to the surface, rather than pointing their active sides toward the substrate. Crucially, by themselves, the active colloids do not cluster or crystallize even under the UV illumination.[17,18]

Although no clustering of active particles is observed, the addition of size-matched inactive silica particles introduces interactions between the different particle species which ultimately lead to the dynamic self-assembly of the active–passive mixture. A typical sequence of images showing the evolution of active clusters under UV illumination is shown in **Figure 2**a–e (see also Video S2 in the Supporting Information). In this case, the particle fraction is only $\phi_p \approx 8\%$ passive colloids, and a mere $\phi_a \approx 0.4\%$ of active particles. The distribution of cluster sizes progresses with time until almost all particles have been collected. It is possible to discern four stages of the assembly process: i) bare active particle propulsion, ii) nucleation of passive particles around asymmetric active cores, iii) active particle symmetrization accompanied by cluster growth, and iv) fusion of individual active clusters by oriented attachment. The entire self-assembly is controllable and reversible through the UV illumination: when the light is switched off (Figure 2f), the clusters melt as Brownian diffusion takes over.

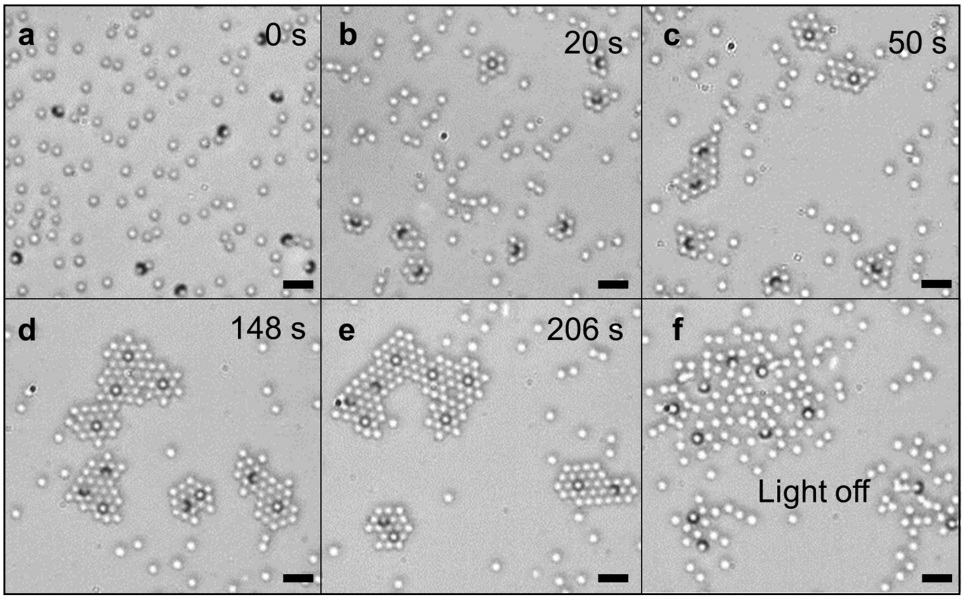

Figure 2. Light-controlled crystal formation in a mixture of active–passive particles (ϕ_a = 0.4%, ϕ_p = 8% in aqueous 1.5% H_2O_2 solution, under light intensity of 320 mW cm^{-2}). a–e) A sequence of images showing the growth of crystals under full UV illumination. Active particles can be distinguished from the passive ones by the dark crescent or ring at their edge. f) Crystals melt by thermal diffusion when the light is turned off (image acquired 12 s after the UV illumination was extinguished). Scale bar indicates 5 μm.

The solution pH has an important effect on the propulsion direction of the Janus particles and the clustering of passive particles around them: at low pH ≈ 4.5 the Janus particles move toward their SiO_2 face (see Figure S2d in the Supporting Information). This behavior has been attributed in other systems to changes in the phoretic mobility.[42] Importantly, under low pH conditions passive particle attraction is not observed; this is consistent with a reversal of the phoretic mobility on SiO_2 relative to neutral pH conditions, which causes the SiO_2 particles to be repelled by the Janus particles. The experiments presented here are all conducted at near neutral pH under conditions that favor passive particle attraction. In addition to SiO_2, we have also driven the assembly of passive particles composed of TiO_2 and NH_2 surface-functionalized SiO_2 (see Figure S5 in the Supporting Information).

Upon UV illumination the active particles' behavior is initially unaffected by the distant passive particles. But this changes when they come into close proximity with one of the passive particles. When an active particle meets a passive one, an attractive interaction binds the two together. This retards straight-line propulsion and causes a small drop in speed. Rapid accumulation of more passive particles follows and they begin to form a planar close-packed shell around the active nucleus. We observe no cases of binding between active particles or passive particles which are not mediated by a particle of the opposite species. The mechanism for attraction is believed to be the same diffusiophoretic interaction that has been observed in other catalytic systems.[40,46] To illustrate the importance of UV intensity on attraction, we have measured the attractive interaction exerted by active particles immobilized to the substrate. **Figure 3**a shows the radial velocity profiles of nearby 1.5 μm passive colloids at three different UV light intensities. It is based on the time evolution of the radial position of infalling particles shown as the inset to Figure 3a. The velocity is well described by $a \propto r^{-2}$ relationship typical for diffusiophoresis. The key feature is that the strength of the attraction can be controlled through the UV intensity (Figure 3b).

When freely propelling, the symmetry axis of the active particles lies in a plane parallel to the surface; this remains true for small crystallites, at least initially, and leads to interesting phenomena which influence the process of large-area self-assembly of the particles. **Figure 4** follows a typical active particle and the small cluster it nucleates. Initially (Figure 4a,b), the active particle travels ballistically before colliding with and collecting a small number of passive particles (Figure 4c,d). Once the nucleation process has begun, two important effects become apparent: first, the passive particles accrete predominantly at the TiO_2 side of the Janus particle; second, the cluster collectively propels, but in the direction away from the TiO_2 face of the active particle, i.e., in the direction opposite that of the bare particle. The asymmetric aggregation arises simply because the diffusiophoretic center of attraction is located toward the TiO_2 reaction site. Once the passive particles are in contact with, and stationary with respect to, the TiO_2, the osmotic flow over the SiO_2 face of the Janus particle is opposed by a counter flow over the attached passive particles. The net result is a reversal of thrust and propulsion of the cluster toward the SiO_2 face of the active particle (see Figure S6 in the Supporting Information for simulations). Similar direction reversal has been predicted for pairs of uniform active particles of mismatched sizes.[47] Importantly, further growth of larger clusters is facilitated by the enhanced diffusion of the asymmetric clusters. The active Janus colloids continue to propel the assembly so that the clusters can collect more particles, even though the number density of active and passive particles is very low (see Figure 4i).

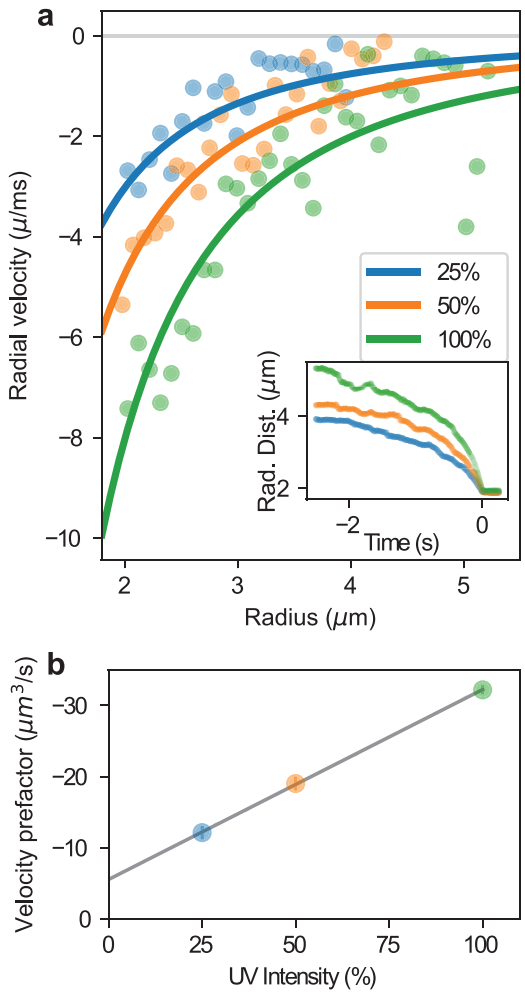

Figure 3. Active–passive particle interaction strength controlled by UV intensity. a) The radial velocity profiles of 1.5 μm passive particles as a function of center-to-center distance from the active attractor at 100% (green), 50% (orange), and 25% (blue) UV light intensity. Full power corresponds to 320 mW cm^{-2}. The lines are fits to the measurements of the form $v = \alpha/r^2$ typical for diffusiophoretic attraction, where the prefactor α is a function of the UV power. The inset shows the mean radial position of many particles from which the main plot is derived by differentiation. b) The prefactors found by fitting show a linear trend in the interaction strength with the light intensity.

The active particle that forms the nucleus of a cluster does not maintain this asymmetric orientation indefinitely. As the first shell fills, most active particles reorient from their tilted configuration (Figure 4e,f) to a symmetric one, where the TiO_2 surface either faces up or down (Figure 4g,h). At long times, over 85% of all active particles undergo this reorientation (see Figure S3 in the Supporting Information). This is generally accompanied by completion of the first shell of passive particles, and is consistent with a radially symmetric osmotic pressure exerted by the passive shell on the active particle it surrounds. At maximum UV intensity, individual clusters grow in size up to two complete hexagonal shells totaling 18 passive particles (6 in the inner shell and 12 in the outer shell) around the central active particle (see the inset in Figure 4h).

Broadly speaking, a regular isolated cluster can be described by its shape (the number of sides) and its size (the number of shells). We show here that we can control both. The first shell shape of a cluster is determined by the contact distances between the passive shell and active nucleus, and between the adjacent passive shell particles. Thus, the size ratio between the active and passive particles r_p/r_a can be used to tune to the clusters' symmetry. Simple geometrical arguments predict the optimal ratio necessary for a cluster with N sides as $r_p/r_a = 2\left(1-\cos\left(\frac{2\pi}{N}\right)\right)$ (see Note 2 in the Supporting Information for details). The ratio comes out to be 2.0, 1.4, 1.0, and 0.75 for square, pentagonal, hexagonal, and heptagonal symmetries, respectively. Furthermore, since the light intensity controls the photochemically driven reaction rate, it can be used to regulate the strength of diffusiophoretic interaction between the active and passive particles. So, by decreasing the UV intensity below the threshold required for stable second-shell aggregation it is possible to capture only first shell passive particles and thus define the cluster's size (see Video S3 in the Supporting Information). **Figure 5** (see also Video S4 in the Supporting Information) shows the effect of cycling between UV intensity of 5 and 30 mW cm^{-2}. High intensity can capture two complete shells around the active particle. When the intensity is reduced, the interaction strength is insufficient to maintain the second shell, and the cluster shrinks as the released passives are stripped away by Brownian diffusion. The process is reversible. **Figure 6** shows rationally constructed single-shell clusters formed by combining these approaches: the clusters' symmetries are determined by the active–passive size ratios and the light intensity has been tuned to limit the agglomeration to one shell.

At high UV intensity, clusters grow beyond a single shell and the average translational speed of clusters shows a smooth decrease as the cluster size grows (Figure 4i for hexagonal clusters). This is consistent with an object growing in hydrodynamic radius but experiencing a fixed propulsive force. Notably, however, the speed remains finite, and this continues even as the clusters grow to their maximum size. We attribute this to microscopic asymmetries in the cluster arrangement or the surface properties of the constituent particles. The net result is that while the average speed of clusters slows, it is always higher than what would be observed in a purely diffusive Brownian system. This facilitates the next stage of assembly: growth of extended crystals.

Once a cluster has two shells filled, it ceases to stably accrete more passive particles, even at the highest UV power at our disposal. Globally however, the growth process continues through the fusion of neighboring clusters by oriented-attachment. As discussed above, the clusters remain motile, propelled by their active core, and this plays an important role in their aggregation by accelerating the rate at which distant clusters approach each other and fuse. In a Brownian scenario, such fusion events would be rare and the chance of observing them very small. Figure S4 (Supporting Information) shows how widely separated hexagonal clusters move into close proximity, reorient and, once the lattices are aligned, fuse (see also Video S5 in the Supporting Information). The cluster symmetry, determined by the particle size ratio, is crucial in deciding which

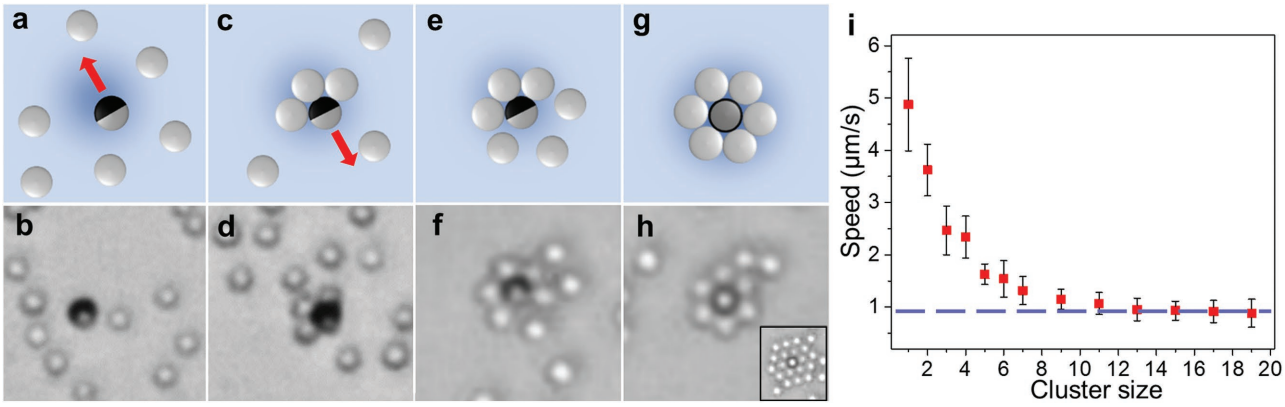

Figure 4. Growth of the first shell. a,b) Under UV illumination, an active particle adopts a tilted orientation, and moves with its TiO_2 face leading. c,d) Once trapped, passive particles preferentially attach to the TiO_2 half (black region), and the active particle's direction of propulsion reverses so that it moves toward its SiO_2 face. The red arrow indicates the moving direction. e–h) When more passive particles attach, the active particle usually reorients into a symmetric configuration with the active TiO_2 surface facing up or down. Once the active particle has reoriented, more passive particles join and completely fill the first shell. The Inset to panel (h) shows an image of a fully grown cluster at maximal UV intensity with two complete shells trapping 18 passive particles. i) The average speed of different size crystals formed around single active particles. The speed decreases monotonically, but is asymptotic and converges to ≈1 μm s^{-1} (blue dashed line) even for very large crystals.

clusters form organized extended crystals with translational periodicity. As expected, clusters with hexagonal and tetragonal symmetry can form close-packed crystals (**Figure 7**a,d). On the other hand, since regular pentagons and heptagons do not tessellate, clusters with these symmetries coalesce into amorphous assemblies (Figure 7b; see Video S6 in the Supporting Information).

The case of tetragonal symmetry is particularly interesting. Here the same ratio of active and passive particles can, depending on the light intensity, lead to large-area crystals or disordered assemblies. At higher intensity, more passive colloids are attracted to the initial clusters and so disrupt the square symmetry (see Figure 7c). However, at intermediate light intensity the growth of the assembly proceeds by piecewise assembly of square clusters yielding a perfect crystal with a square lattice (see Figure 7d and Video S7 in the Supporting Information).

In summary, we have demonstrated the dynamic self-assembly of colloids driven by a small population of active particles. The active particles act as mobile nucleation centers that condense the sparsely distributed passive particles, and

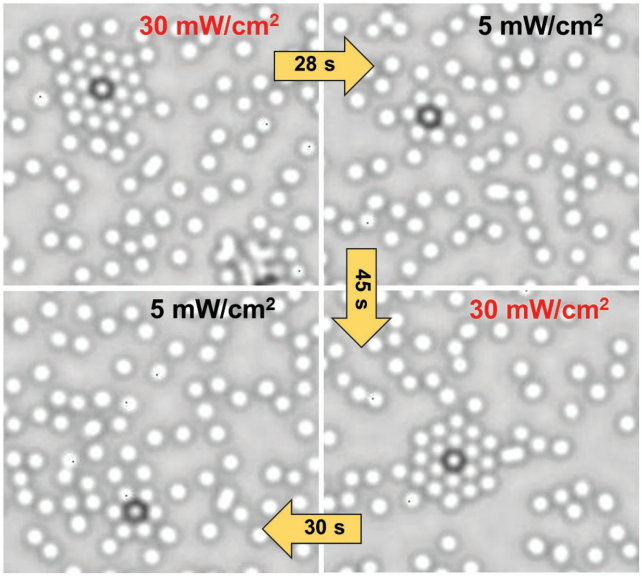

Figure 5. Light-controlled tunability of the cluster size. Two cycles of reversible size modulation of a hexagon cluster by controlling the light intensity is shown. The time between the frames is labeled on the arrows.

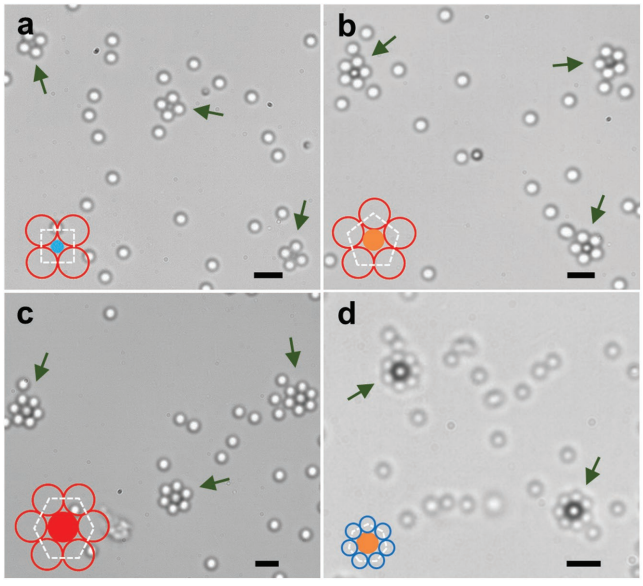

Figure 6. Symmetry of active clusters determined by the active–passive particle size ratio. Self-assembled single-shell clusters formed at low light intensity (≈5 mW cm^{-2}): a) square, b) pentagon, c) hexagon, and d) heptagon. Schematics show the size and position of active/passive particles. The open and closed circles represent the passive and active particles, respectively, while the colors represent their sizes; blue, orange, and red are for 1.0, 1.5, and 2.1 μm, respectively. The green arrows are indicating the formed clusters. Scale bar indicates 5 μm.

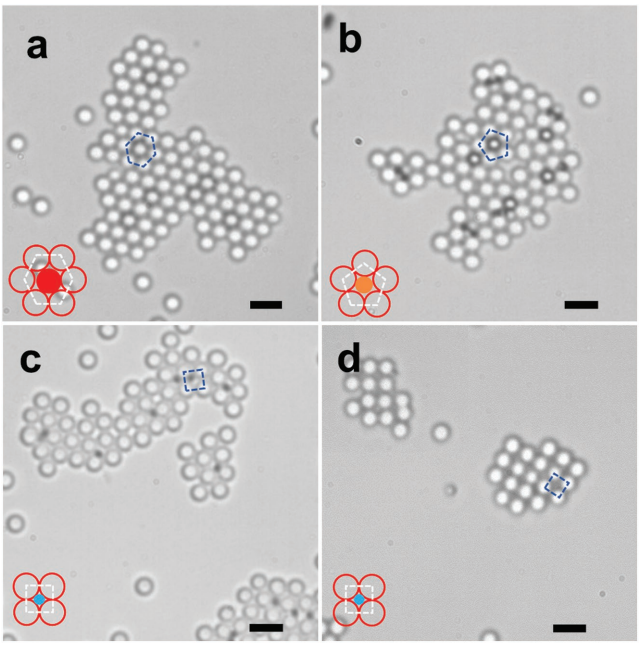

Figure 7. Extended assemblies of active–passive mixtures at high light intensity. Passive colloids are 2.1 μm in diameter for all examples. a) Hexagonal lattice formed with size-matched 2.1 μm active particles. b) Disordered glass formed with pentagonal units (active particle size 1.5 μm). Panels (c) and (d) show the disordered and square lattice clusters formed with the same size active particles (1 μm). At maximal UV intensity, the square-shaped small cluster units form disordered arrangements. However, at reduced light intensity, such that only a single shell can form around an active nucleus, increased passive particle mobility allows improved square lattice order. The unit cluster around an active particle with a single shell of passive colloids is highlighted by the dashed color lines. Scale bar indicates 5 μm.

drive the enhanced diffusion of small clusters. Compared with conventional equilibrium system, where colloidal assembly is kinetically limited and typically a slow process, the present non-equilibrium active colloidal system leads to rapid clustering at very low densities. The shape and size of individual small clusters as well as the lattice order of the large cluster they form after fusion can be easily changed by controlling the light intensity and size ratio of active–passive particles. This dynamic self-assembly approach can be used to fabricate 2D colloidal glasses or crystals of different lattices. Since the activity of the system is triggered by light, it is possible to easily switch between crystal growth and melting. In our system, the growth dynamics allow facile optical observation of the attachment, alignment, and reorientation of clusters, and fusion during the growth. These macroscopic observations could be interesting to understand 2D atomic or molecular crystallization where oriented-attachment of nanoscale crystallites play an important role.[48–51] It should also be possible to exert external motion control over the clusters using, for instance, magnetized particles in an external magnetic field. We expect that these multicomponent active–passive systems can go beyond traditional colloidal systems by opening up a route to new structures and assemblies that cannot be obtained in purely passive systems.

Experimental Section

Fabrication of Active Janus Particles: We started with commercial SiO_2 microspheres (Micromod) of 2.1, 1.5, or 1 μm. These are made hydrophobic by surface functionalization with allyltrimethoxysilane and dispersed in chloroform. This suspension was spread over the surface of the water subphase in a Langmuir–Blodgett trough and the resulting monolayer was transferred onto a Si wafer at a surface pressure of ≈20 mN m^{-1}.[52] The substrate supported monolayers were transferred to the vacuum system where a 60 nm TiO_2 film was deposited by e-beam evaporation at normal incidence. After deposition, the Janus particles were annealed at 450 °C for 2 h in air. X-ray diffraction confirmed the presence of the anatase phase (see Figure S1 in the Supporting Information for XRD pattern). Prepared Janus particles were detached from the Si substrate by sonication in water.

Propulsion of Active Janus Particles: Active particle propulsion and crystal formation were observed in an aqueous solution of 1.5 % hydrogen peroxide and 1×10^{-3} M tetramethylammonium hydroxide (TMAH). The TMAH was added to adjust the pH of the solution to keep it approximately neutral. Control experiments to test the activity of Janus particles in TMAH with and without H_2O_2 indicate that TMAH does not undergo photocatalytic decomposition (see Figure S2 in the Supporting Information). The propulsion arises from the photo-decomposition of H_2O_2 at the TiO_2 surface of Janus particles under UV illumination.

Illumination and Observation: The samples for observation were prepared by mixing active and passive particles with the reactant solution immediately before use. A sessile droplet of the mixture, supported by a glass cover slip and exposed to air, was imaged from the underside. The particles in the droplet were allowed to sediment before experiments began. Microscopy images were captured using a 50× 0.55NA objective in an inverted geometry. A UV light emitting diode served as the light source for TiO_2 excitation in an epifluorescence-type arrangement. The maximum UV intensity was 320 mW cm^{-2} in the sample plane. The discrete clusters shown in Figure 6 were formed by accreting an excess of passive particles around an active core and then reducing the UV intensity to a level sufficient to stably bind only a single shell. Image acquisition rates ranged from 8 to 200 fps. For the measurements of speed, the clusters were tracked for a minimum of 20 s; particle trajectories were identified and refined with the ImageJ distribution Fiji and plugin TrackMate.[53]

The interaction potential illustrated in Figure 3a was collected by first drying 2.1 μm active particles onto the glass substrate to immobilize them before adding dispersed 1.5 μm passive colloids. The collection of passive particles was observed at 200 fps at 100%, 50%, and 25% UV intensity. The trajectories of the passive particles were identified with the Python package Trackpy.[48] The time evolution of the infalling particles shown as the inset to Figure 3a was calculated from the mean of 20 to 30 particle trajectories at each light level.

Numerical Simulations: Finite element simulations of local concentration were conducted using the "transport of diluted species" module of COMSOL Multiphysics. The particle diameters were 1.5 μm. The hemispherical active surface of the Janus particle was modeled as a source of solute with a flux of 1 mmol m^2 s^{-1}. A fixed solute flux is consistent with reaction kinetics in the limit of large solute substrate concentration and low solute product concentration. The diffusion constant of O_2 in water is 2.1×10^{-9} m^2 s^{-1}. The particles lay upon an inert substrate. A gap of 100 nm was allowed between the particles and substrate and between the particles to ensure convergence. A surrounding "infinite element domain" was used to simulate isolated particles and clusters.

Supporting Information

Supporting Information is available from the Wiley Online Library or from the author.

Acknowledgements

The authors are grateful to E.J. Mittemeijer and P. Rossi for XRD measurements. The authors thank C. Miksch for preparing Langmuir–Blodgett (LB) films. The authors thank A. Ghosh for helpful comments. This work was supported by the DFG as part of the project SPP 1726 117 (microswimmers, FI 1966/1-1), and the Max Planck Society.

Conflict of Interest

The authors declare no conflict of interest.

Keywords

dynamic assembly, light-driven motors, Janus particles, self-assembly, self-propulsion

Received: March 8, 2017
Revised: April 8, 2017
Published online: June 20, 2017

[1] E. Winfree, F. Liu, L. A. Wenzler, N. C. Seeman, *Nature* **1998**, *394*, 539.
[2] Y. Tian, Y. Zhang, T. Wang, H. L. Xin, H. Li, O. Gang, *Nat. Mater.* **2016**, *15*, 654.
[3] Y. Wang, Y. Wang, D. R. Breed, V. N. Manoharan, L. Feng, A. D. Hollingsworth, M. Weck, D. J. Pine, *Nature* **2012**, *491*, 51.
[4] D. Manna, T. Udayabhaskararao, H. Zhao, R. Klajn, *Angew. Chem., Int. Ed.* **2015**, *54*, 12394.
[5] S. Ni, J. Leemann, I. Buttinoni, L. Isa, H. Wolf, *Sci. Adv.* **2016**, *2*, e1501779.
[6] S. Das, P. Ranjan, P. S. Maiti, G. Singh, G. Leitus, R. Klajn, *Adv. Mater.* **2013**, *25*, 422.
[7] H. P. Zhang, A. Be'er, E.-L. Florin, H. L. Swinney, *Proc. Natl. Acad. Sci. USA* **2010**, *107*, 13626.
[8] M. C. Marchetti, J. F. Joanny, S. Ramaswamy, T. B. Liverpool, J. Prost, M. Rao, R. A. Simha, *Rev. Mod. Phys.* **2013**, *85*, 1143.
[9] A. Cavagna, I. Giardina, *Annu. Rev. Condens. Matter Phys.* **2014**, *5*, 183.
[10] X. Chen, X. Yang, M. Yang, H. P. Zhang, *Europhys. Lett.* **2015**, *111*, 54002.
[11] A. P. Petroff, X.-L. Wu, A. Libchaber, *Phys. Rev. Lett.* **2015**, *114*, 158102.
[12] T. Ishikawa, M. Hota, *J. Exp. Biol.* **2006**, *209*, 4452.
[13] N. C. Darnton, L. Turner, S. Rojevsky, H. C. Berg, *Biophys. J.* **2010**, *98*, 2082.
[14] A. Finkelshtein, D. Roth, E. Ben Jacob, C. J. Ingham, *mBio* **2015**, *6*, e00074.
[15] A. Bricard, J.-B. Caussin, N. Desreumaux, O. Dauchot, D. Bartolo, *Nature* **2013**, *503*, 95.
[16] M. Ibele, T. E. Mallouk, A. Sen, *Angew. Chem., Int. Ed.* **2009**, *48*, 3308.
[17] J. Palacci, S. Sacanna, A. P. Steinberg, D. J. Pine, P. M. Chaikin, *Science* **2013**, *339*, 936.
[18] I. Buttinoni, J. Bialké, F. Kümmel, H. Löwen, C. Bechinger, T. Speck, *Phys. Rev. Lett.* **2013**, *110*, 238301.
[19] W. Wang, W. Duan, S. Ahmed, A. Sen, T. E. Mallouk, *Acc. Chem. Res.* **2015**, *48*, 1938.
[20] O. Pohl, H. Stark, *Phys. Rev. Lett.* **2014**, *112*, 238303.
[21] A. Zöttl, H. Stark, *J. Phys. Condens. Matter* **2016**, *28*, 253001.
[22] J. Yan, M. Han, J. Zhang, C. Xu, E. Luijten, S. Granick, *Nat. Mater.* **2016**, *15*, 1095.
[23] J. Stenhammar, R. Wittkowski, D. Marenduzzo, M. E. Cates, *Sci. Adv.* **2016**, *2*, e1501850.
[24] W. Gao, A. Pei, R. Dong, J. Wang, *J. Am. Chem. Soc.* **2014**, *136*, 2276.
[25] J. R. Howse, R. A. L. Jones, A. J. Ryan, T. Gough, R. Vafabakhsh, R. Golestanian, *Phys. Rev. Lett.* **2007**, *99*, 048102.
[26] T.-C. Lee, M. Alarcón-Correa, C. Miksch, K. Hahn, J. G. Gibbs, P. Fischer, *Nano Lett.* **2014**, *14*, 2407.
[27] Y. Mei, A. A. Solovev, S. Sanchez, O. G. Schmidt, *Chem. Soc. Rev.* **2011**, *40*, 2109.
[28] U. Choudhury, L. Soler, J. G. Gibbs, S. Sanchez, P. Fischer, *Chem. Commun.* **2015**, *51*, 8660.
[29] Z. Wu, Y. Wu, W. He, X. Lin, J. Sun, Q. He, *Angew. Chem., Int. Ed.* **2013**, *52*, 7000.
[30] W. Gao, A. Pei, X. Feng, C. Hennessy, J. Wang, *J. Am. Chem. Soc.* **2013**, *135*, 998.
[31] W. Wang, W. Duan, A. Sen, T. E. Mallouk, *Proc. Natl. Acad. Sci. USA* **2013**, *110*, 17744.
[32] R. Ni, M. A. Cohen Stuart, M. Dijkstra, P. G. Bolhuis, *Soft Matter* **2014**, *10*, 6609.
[33] J. Stenhammar, R. Wittkowski, D. Marenduzzo, M. E. Cates, *Phys. Rev. Lett.* **2015**, *114*, 018301.
[34] F. Mou, Y. Li, C. Chen, W. Li, Y. Yin, H. Ma, J. Guan, *Small* **2015**, *11*, 2564.
[35] I. Ilisz, K. Föglein, A. Dombi, *J. Mol. Catal. Chem.* **1998**, *135*, 55.
[36] P. Salvador, F. Decker, *J. Phys. Chem.* **1984**, *88*, 6116.
[37] R. Dong, Q. Zhang, W. Gao, A. Pei, B. Ren, *ACS Nano* **2016**, *10*, 839.
[38] F. Mou, L. Kong, C. Chen, Z. Chen, L. Xu, J. Guan, *Nanoscale* **2016**, *8*, 4976.
[39] J. G. Gibbs, Y. Zhao, *Small* **2010**, *6*, 1656.
[40] J. Palacci, S. Sacanna, S.-H. Kim, G.-R. Yi, D. J. Pine, P. M. Chaikin, *Philos. Trans. R. Soc., A* **2014**, *372*, 20130372.
[41] C. Chen, F. Mou, L. Xu, S. Wang, J. Guan, Z. Feng, Q. Wang, L. Kong, W. Li, J. Wang, Q. Zhang, *Adv. Mater.* **2017**, *29*, 1603374.
[42] A. Brown, W. Poon, *Soft Matter* **2014**, *10*, 4016.
[43] J. Simmchen, J. Katuri, W. E. Uspal, M. N. Popescu, M. Tasinkevych, S. Sánchez, *Nat. Commun.* **2016**, *7*, 10598.
[44] S. Das, A. Garg, A. I. Campbell, J. Howse, A. Sen, D. Velegol, R. Golestanian, S. J. Ebbens, *Nat. Commun.* **2015**, *6*, 8999.
[45] S. Ebbens, D. A. Gregory, G. Dunderdale, J. R. Howse, Y. Ibrahim, T. B. Liverpool, R. Golestanian, *Europhys. Lett.* **2014**, *106*, 58003.
[46] J. Palacci, S. Sacanna, A. Vatchinsky, P. M. Chaikin, D. J. Pine, *J. Am. Chem. Soc.* **2013**, *135*, 15978.
[47] S. Michelin, E. Lauga, *Eur. Phys. J. E: Soft Matter Biol. Phys.* **2015**, *38*, 7.
[48] J. Baumgartner, A. Dey, P. H. H. Bomans, C. Le Coadou, P. Fratzl, N. A. J. M. Sommerdijk, D. Faivre, *Nat. Mater.* **2013**, *12*, 310.
[49] R. L. Penn, J. A. Soltis, *CrystEngComm* **2014**, *16*, 1409.
[50] D. Li, M. H. Nielsen, J. R. I. Lee, C. Frandsen, J. F. Banfield, J. J. De Yoreo, *Science* **2012**, *336*, 1014.
[51] J. Fang, B. Ding, H. Gleiter, *Chem. Soc. Rev.* **2011**, *40*, 5347.
[52] D. Schamel, M. Pfeifer, J. G. Gibbs, B. Miksch, A. G. Mark, P. Fischer, *J. Am. Chem. Soc.* **2013**, *135*, 12353.
[53] C. A. Schneider, W. S. Rasband, K. W. Eliceiri, *Nat. Methods* **2012**, *9*, 671.